[American Journal of Science, Vol. 307, September, 2007, P. 955–973, DOI 10.2475/07.2007.01]

American Journal of Science

SEPTEMBER 2007

CONVERGED SURFACE ROUGHNESS PARAMETERS—A NEW TOOL TO QUANTIFY ROCK SURFACE MORPHOLOGY AND REACTIVITY ALTERATION

CORNELIUS FISCHER*,**,† and ANDREAS LÜTTGE*,§

ABSTRACT. The quantification of surface topography is essential in understanding the processes of dissolution and precipitation occurring at the rock-water interface. As a new approach to quantify rock surface alteration in the micrometer to nanometer scale we utilize the convergence of well-known surface roughness parameters. This approach allows the quantification of rock surface size and amplitude as well as its state of alteration during fluid-rock interaction. Vertical scanning interferometry (VSI) is our tool of choice for measuring rock surface topography because of its high vertical resolution and large field of view.

Here, we present a case study to demonstrate the potential of surface roughness convergence for quantifying rock surface alteration during weathering. Black slates show different concentrations of organic matter (OM) due to different oxidative weathering ranks. Roughness and surface size data indicate that the original smooth slate surface with deviations of only some tens of nanometers was altered to a rough surface with pore diameters at a scale of some hundreds of nanometers up to several microns. Surface roughness data of a sample profile of three weathering stages (small, medium, large OM decrease) primarily indicate an increase of the OM's surface area and roughness during weathering. However, during further weathering, surface area and roughness were decreased. From these data we conclude that those parts of the OM that do not directly adjoin to the slate's clay minerals have a higher reactivity. This means that during ongoing OM weathering the rock surface reactivity and topography are controlled by the extent of OM degradation. Because both reactivity and topography of the observed surface will alter during reaction, it must be concluded that a constant term of "reactive" surface area must not be used to calculate the dissolution rates.

INTRODUCTION

The fluid-rock interface alters in size and shape during weathering processes. Most importantly, however, it also changes in reactivity. Hence, the characterization and quantification of surface area evolution are needed to quantitatively understand fluid-rock interactions. The simplest case is the alteration of a single crystal surface. Much laboratory work has been conducted over decades to reconstruct those surface changes and to interpret dissolution and precipitation kinetics of single crystals (Eggleton and Busek, 1980; Helgeson and others, 1984; Lasaga and Blum, 1986; Hochella and White, 1990; White and Brantley, 1995). Surface area was measured by AFM methods to calculate surface area changes during reactions (for example, Dove and Platt, 1996; Arvidson and others, 2003; Metz and others, 2005). In contrast, to

*Department of Earth Science, MS-126, Rice University, 6100 Main Street, Houston, Texas 77005, U.S.A.

**Geowissenschaftliches Zentrum der Universität Göttingen, Abt. Sedimentologie and Umweltgeologie, Goldschmidtstrasse 3, D-37077 Göttingen, Germany

§Department of Chemistry, Rice University, 6100 Main Street, Houston, Texas 77005, U.S.A.

†Corresponding author, e-mail: cornelius@rice.edu

detect and quantify the results of dissolution processes occurring in mineral aggregates and rocks it is necessary to determine surface area changes over a significantly larger field of view than AFM can provide.

More recently, vertical scanning interferometry (VSI) (for example, Lüttge and others, 1999) and confocal laser scanning microscopy (LSM) (Karcz and others, 2006) have been developed as new tools to distinguish and trace the reactive parts of mineral surfaces. LSM and VSI are complementary techniques and particularly well suited to detect surface changes within a large field of view. The LSM technique provides a superior lateral ($\sim$ 100 nm) but lower vertical resolution than VSI. However, a simple application of such results to the significantly more complex natural fluid-rock system is often difficult or even impossible because of the chemical, physical, and hydraulic permeability properties [connected/unconnected porosity, pore size (for example IUPAC, 1994; Lion and others, 2004)].

In industrial production processes, VSI techniques are widely used for characterizing and testing the machine finished surfaces of work pieces. As a result, a number of statistical surface parameters have been established over decades to quantify the information obtained from surface area measurements conducted by 2D or 3D "large-area" techniques (Dong and others, 1992, 1993, 1994a, 1994b; Stout, 1993; Blunt and others, 2005). Our attempt here is to adapt these roughness parameters to the characterization and quantification of rock surface alteration caused by weathering.

Dissolution and precipitation processes during weathering change the fluid-rock interface properties through the formation of, for example, pores and secondary minerals. Therefore, a crucial step for surface and reactivity quantification is to explore how different surface components impact roughness parameters over a range of vertical and lateral scales. Consequently, it is preferable to compare the surface roughness parameters as a function of different sizes of the field of view.

Based on our insight above, the study presented here has two main objectives: First, we show the ability to characterize and quantify natural rock surfaces by converged statistical surface roughness parameters. Second, we will try to trace the surface evolution of rocks during weathering with these parameters. For this purpose we will compare surface roughness parameters of rocks showing different stages of weathering.

Numerical Parameters for Characterization of Surface Topography

A 3D data set of a given sample surface is built up of several superimposing surface components of different sizes. From the common material science point of view, the measured surface consists of three superimposing units: (I) the form surface is the shape of the work piece. (II) low-frequency and (III) high-frequency deviations from this shape may occur. These deviations result in the so-called surface waviness and roughness. This classification is not useful to describe natural surfaces because we usually do not know if there are only two classes of surface deviations and what the discrimination size between the surface features (or wavelength of component size) is. Therefore, we suggest the use of convergence for the application of surface roughness parameters and introduce convergence graphs of roughness parameters. We will apply convergence graphs for three different amplitude parameters and a surface area parameter. We characterize surface topography by using sets of numerical parameters derived from statistical calculations of surface deviations. The so-called *S*-parameter set contains 15 parameters of different types [amplitude, spacing, hybrid, fractal dimension parameters (Blunt, 2003)]. To characterize surface area changes during chemical rock alteration, we utilize the peak-to-valley depth (Rt), ten-point peak-to-valley average depth (Rz), root-mean-square deviation of the surface (Rq), and interfacial area ratio (F). Below, we give a short explanation for the calculation of these surface topographic parameters (Jorgensen and others, 1993).

The height difference between the pixel with the highest and the lowest z value in a surface height map is the peak-to-valley depth

$$Rt = z_{\max} - z_{\min}. \tag{1}$$

The ten-point height, *Rz*, is defined as the average height of the five highest (peak) local maxima plus the average height of the five lowest (valley) local minima:

$$Rz = \frac{\sum_{i=1}^{5} (z_{pi} - \mu) + \sum_{i=1}^{5} (z_{vi} - \mu)}{5}, \tag{2}$$

where μ is the mean height given by:

$$\mu = \frac{1}{MN} \sum_{k=0}^{M-1} \sum_{l=0}^{N-1} z(x_k, y_l).$$

z_{pi} and z_{vi} are the height values of the ith highest local maximum and the ith lowest local minimum, respectively.

We present a graph of *Rz* only in cases when the trend shown by this value is significantly different from that shown by *Rt*. In most cases *Rt* and *Rz* show the same trend.

Rq is also an amplitude parameter and is used to describe dispersion of the height distribution. It is the sample standard deviation and describes the deviation of measured surface sites from the mean or another reference surface, for example, a "*zero*" plane. For calculations of *Rq* the surface is considered as a line set of N profiles. Each profile has a number of M points.

$$Rq = \sqrt{\frac{1}{MN} \sum_{k=0}^{M-1} \sum_{l=0}^{N-1} [z(x_k, y_l) - \mu]^2} \tag{3}$$

The amplitude parameter, *Ra*, defines the average surface roughness, that is the arithmetic mean of surface deviations and is often used to trace surface alteration such as corrosion of work pieces (Ayebah and Hung, 2005). However, several studies have shown that no significant information about surface features can be attained by using *Ra* (for example, Thomas, 1999) because similar *Ra* values can be derived from surfaces showing completely different characteristics of their peak and valley configuration.

In contrast, the root mean square average, *Rq*, is more sensitive to minima and maxima of a surface structure due to the squared term (see eq 3). Generally, the utility of amplitude parameters for direct interpretation of surface features is good only for surfaces built up by a periodical structure.

The surface area ratio, *F*, expresses the ratio between the measured surface area, F_m, and the area of the flat xy plane, which is the sampling area, F_0. For a totally flat surface, the total and geometrical surface area and the sampling area are the same ($F = 1$).

$$F = \frac{F_m}{F_0} \tag{4}$$

Surface Topography Parameters and Their Significance for Rock Surface Characterization: Use of Converged Parameters

It can be shown that the usual approach of describing work piece form, waviness, and roughness cannot be used in the characterization of rock surfaces (Thomas, 1999). We cannot hypothesize that a rock surface is formed by the superimposition of so-called surface waviness and roughness. Generally, we find on rock surfaces several components, these are mineral aggregates and pores within a range of sizes. It is clear that this situation results in a mixture of surface roughness values. So, surface parameters such as amplitude and hybrid parameters are not useful in characterizing such surfaces. For example, it would be meaningless to calculate the mean *Rq* values of surfaces with different peak heights, peak diameters, and peak densities. Such a mixture of differently sized surface components, however, would be the expected case for most natural rock surfaces.

Now, we introduce the idea of using converged surface roughness parameters to obtain a deconvolution of surface components of different size scales. Convergence graphs show the variation of a roughness parameter depending on the size of the sampling area. The roughness parameters defined by equations (1) to (4) were first calculated for the entire data set and, subsequently, for increasingly smaller sections of this data set. These sections were produced by a recurrent bisection of the measuring field (fig. 1A). The small axes (a_0-a_n) are the reference values for each plotted roughness parameter to characterize the measuring field size. Converged surface parameters were calculated from partial data sets of the original total data set. Therefore, the spatial resolution (pixels per length scale unit) of all data subsets is identical.

The convergence calculation is determined by two variables (fig. 1B). The number of steps, *n*, for sampling area reduction specifies the precision of the convergence length. The convergence direction within the measured field is important if a surface is non-uniform and you want to know which surface structures were sampled.

We define that a surface parameter is *converged* if neighboring data points of the convergence graph show a flat slope ($df(a)/da$ near 0, *a*: length) in contrast to the adjoining steep-slope sections of the graph. If this criterion is satisfied, then the converged parameter value can be used to characterize and quantify topography of the associated surface section. Converged graphs of *Rt* will rarely show sections of pronounced near-zero slope. The reason is that *Rt* quantifies the maximum height difference of the surface. *Rt* may reflect outlier height data. Therefore, we used at least three data points with near-zero slope to define a converged *Rt* height. Root-mean-square roughness *Rq* does not reflect surface height outliers. Therefore, we used the criterion of at least two neighboring data points with near-zero slope between them to define convergence. The same criterion was applied to the surface area ratio *F* and to *Rz*, which represents the average height of the five highest local maxima plus the average height of the five lowest local minima.

Figure 2 gives an example of convergence graphs of a known surface, a matt-finished glass plate. The surface consists of hills that are approximately 2 to 2.5 μm high and 4 μm wide (peak-to-peak width is approx. 8 μm). Figure 2A shows a section of the (*x,y,z*) data set within a field of view of 30 μm x 40 μm. Figure 2B shows convergence graphs of *Rt*, *Rq*, and *F*. The *Rt*-value graph has a flat slope between ~ 8 μm and 60 μm axis length (maximum height without outlier). The high *Rt* values within the large field of view are caused by scratches in the glass surface. *Rt* is sensitive for the maximum peak height. If the field of view is small enough and no scratches are imaged, *Rt* values indicate only the maximum peak height caused by the glass matting process. If the reduction of our field-of-view is smaller than the peak-to-peak length, the *Rt* convergence is abolished (part ii). The constancy of *Rq* and *F* for medial and

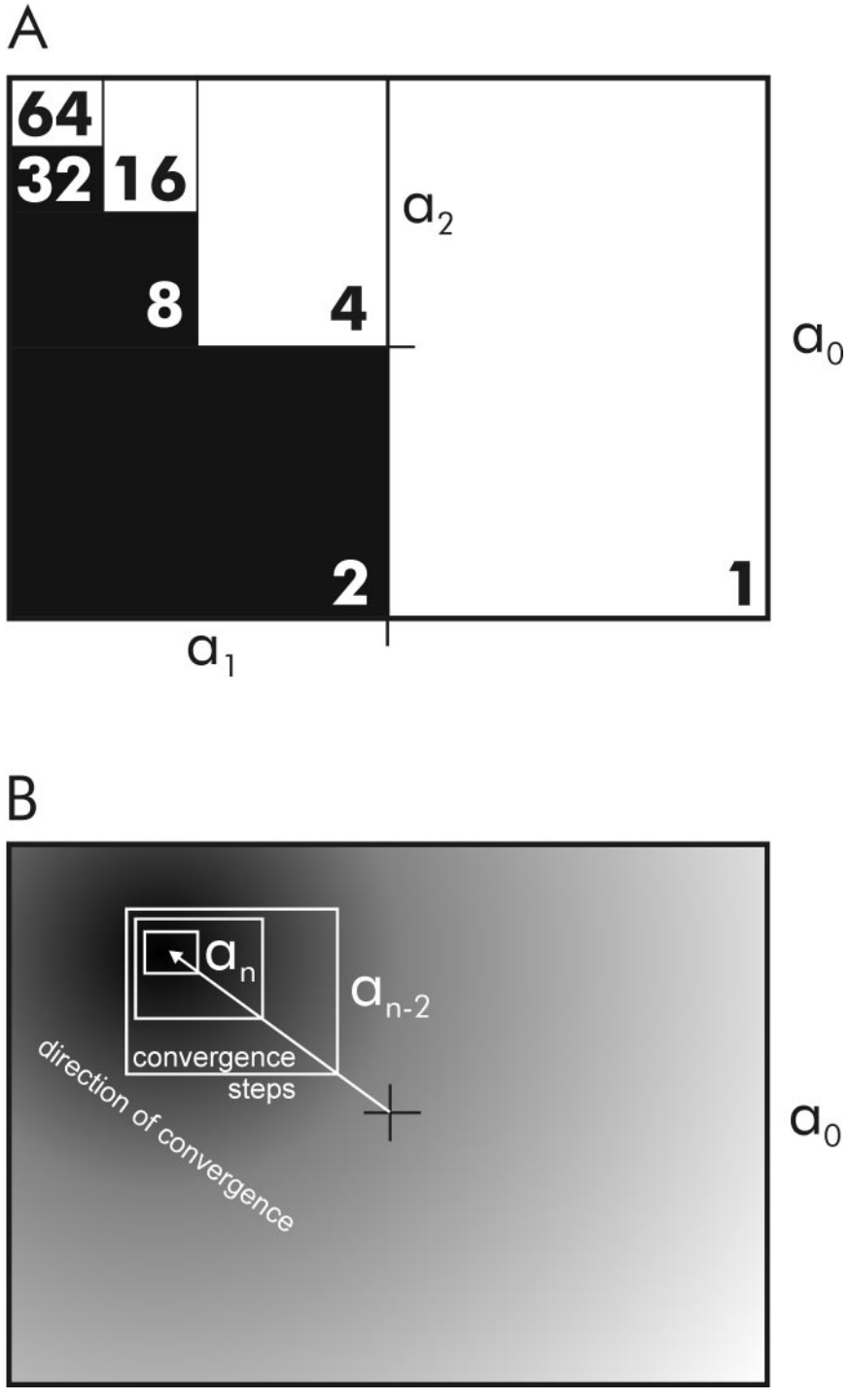

Fig. 1. (A) Measuring field (= $a_0 * 2a_1$) and smaller and smaller sections of the field by a recurrent bisection. (B) Suggestion for a continuously measuring field reduction, characterized by two parameters (direction, step number).

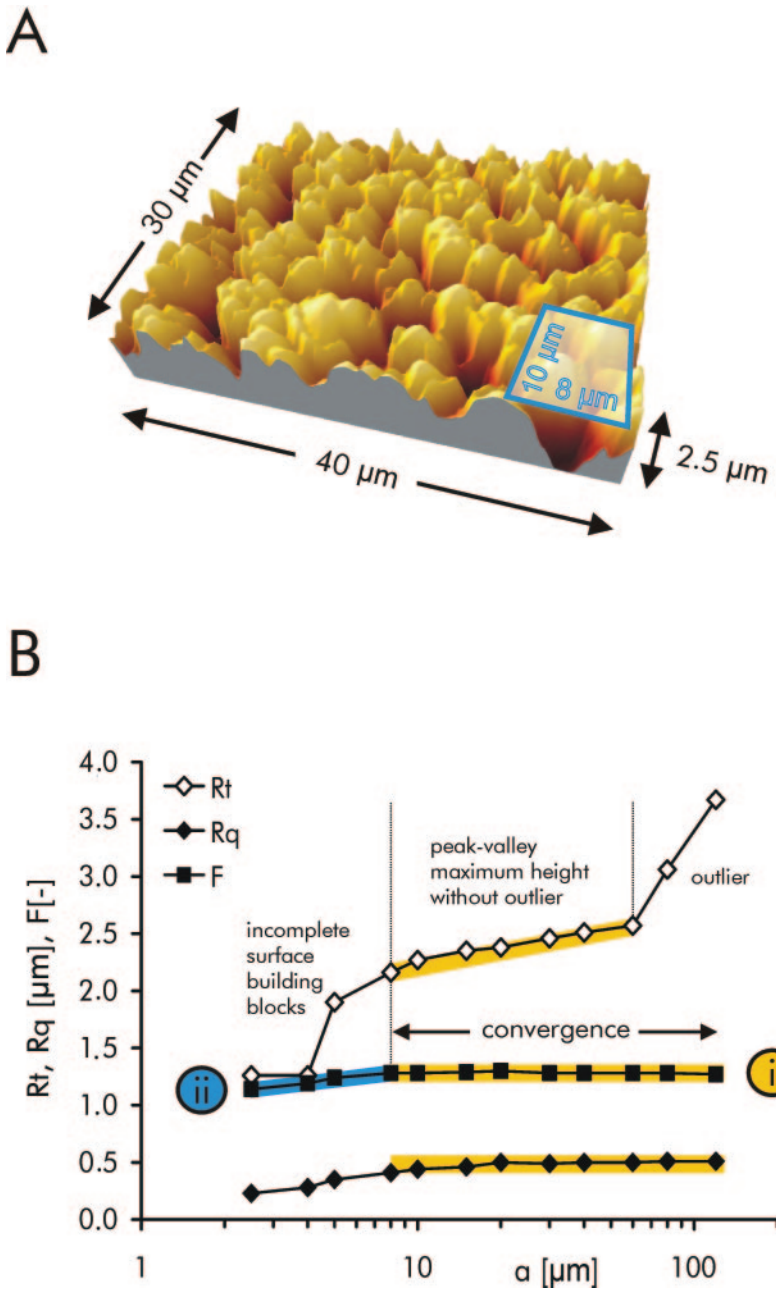

Fig. 2. (A) VSI data of a matt-finished glass slide, size 40 µm * 30 µm. The matt-finished glass shows a structure of hills and valleys. Peak to valley high is approx. 2 to 2.5 µm, peak to peak distance is approx. 8 µm. (B) Convergence of surface roughness (*Rq*) and surface ratio (*F*) are shown over length *a* of measured area. Note the breakdown length of $a = 8$ µm for converged *Rq*, *F* values (border between blue and yellow lines, compare to fig. 2A).

large axis length (part i) demonstrates that only one surface component dominates the surface structure. Two important and differently sized surface components would produce two plateaus in both, the *Rt* and *Rq* graphs. This example illustrates the ability of convergence graphs to distinguish quantitatively between different surface components.

METHODS AND MATERIALS

Surface Area Scanning Methods

Surface area characterization and quantification requires a method that allows a sufficiently high spatial resolution, similar to that provided by atomic force microscopy (AFM) or scanning tunneling microscopy (STM) but also a much larger field of view that is similar to that provided by common light optical microscopy (Stout, 1993). In this study, we have used two different light optical microscopy methods, vertical scanning interferometry [VSI, MicroXAM MP8, ADE Phase Shift; for a detailed description see, for example, Lüttge and others (2003)] and confocal laser scanning microscopy [LSM, ZEISS LSM 510 Meta, EC-Epiplan-Apo 100x 0.95 HD DIC, beam splitters MBS NT80/20, DBS: plate, wavelength = 405 μm, pinhole = 52 μm, 12 bit multi track stack scan mode, sampling area: 92.1 μm x 92.1 μm, scaling 0.09 μm x 0.09 μm x 0.1 μm, pixel time: 0.80 μs]. Three-dimensional surface measurements by confocal scanning microscopy were described by Hamilton and Wilson (1982).

Both light optical methods are capable of providing a field of view of more than 100 μm x 100 μm with a sufficiently high spatial resolution. VSI in combination with a white light source provides resolution in the *z*-direction of better than 2 nm (for example, Lüttge and others, 2003); the resolution of LSM is one or two orders of magnitude lower. The lateral x-y resolution of VSI is approximately 500 nm (for a 50x Mirau objective). In contrast, LSM provides approximately 100 nm. The complementary use of VSI data to LSM is useful, because VSI is not able to detect steeply dipping flanks due to its very different lateral and vertical spatial resolution. Therefore, steep flanks will be interpolated as smooth planes between the detected surface points.

Black Slate Samples with Different Weathering Intensities

For this study, we compared the surface area data of black slates with different degrees of organic matter degradation caused by oxidative weathering. Two types of samples were used: alum slates and black roof slates.

Alum slates.—Freshly mined lower Silurian, low-grade metamorphic black alum slates from Thüringen (Germany) contain approximately 6 to 15 weight percent organic carbon (TOC). The slate is composed mainly of the clay mineral, illite, and, in part, of minor amounts of microquartz caused by diagenetic silification of recrystallized material from microfossils. Due to weathering processes the slate may release up to 90 percent of its TOC. In addition, sulfide oxidation may cause an iron rich encrustation of the sample surface. We studied a black sample (#211) that was rich in organic matter (OM), [C_{org} = 11.8 wt%] and a weathered sample of white slate from the same location that was nearly free of TOC (sample #224, C_{org} = 0.2 wt%). Both samples were free of iron rich encrustations. In addition, a sample profile of the same slate type was investigated at the millimeter scale with three profile points (black, gray, and white). Here the TOC decreases from the black colored part (TOC ~ 8 wt%) to the gray colored area (TOC ~ 2 wt%) and the white colored (TOC ~ 1.4 wt%) section of the profile. Our black slate samples were free of sulfides because of the fast dissolution rates of sulfides during oxidative weathering. This explanation is supported by, for example, Littke and others (1991) for other black pelites. Due to the lack of sulfides, our comparison of rock surfaces is not influenced by a pore space alteration during sulfide weathering (for a more detailed sample description and location map see Fischer and Gaupp, 2005).

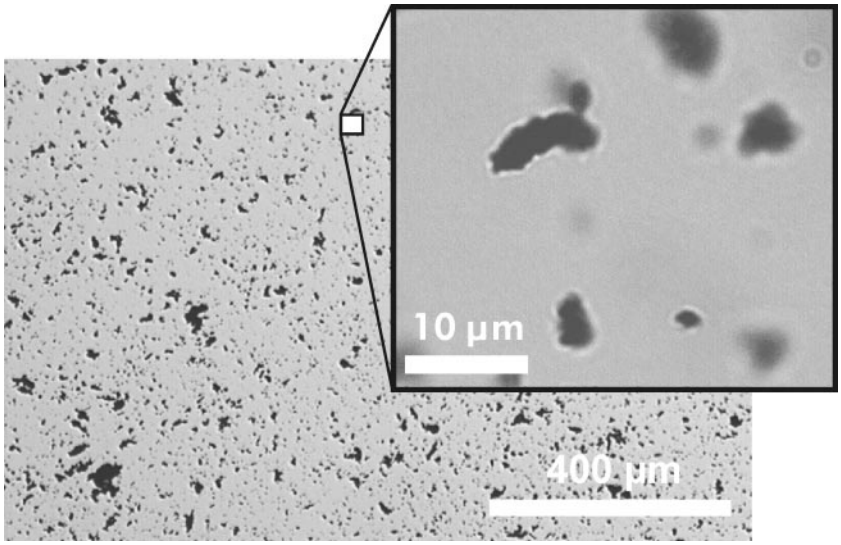

Fig. 3. Size distribution of organic matter flakes from black alum slates.

Roof slates.—Fresh, unbleached Lower Carboniferous (Visean) black roof slate (Pfeiffer and others, 1995) from the Schmiedebach-Lehesten mine (samples #399 and #401) as well as used and weathered roof slate (samples #370, #378, and #379) were investigated for this study. The average mineralogical composition of the freshly mined Lehesten slate shows quartz (41 wt%), illite (35 wt%), chlorite (17.5 wt%), plagioclase (6 wt%), and pyrite (0.5 wt%) (Rothenhöfer and others, 1999); however, this study did not report the slate's organic carbon content. The mercury intrusion porosity of fresh mined slates is 0.2 weight percent (sample #399) and 0.7 weight percent (sample #401). During the weathering of sample #379, its porosity increases up to 1.3 weight percent (black part) and 3.1 weight percent (white margin) (Fischer and Koch, 2005).

The slates used for analyses were exposed for (i) 94 years at a southerly oriented house wall (sample #379), (ii) for 90 years at a westerly exposed house wall (#378) in the Thüringisches Schiefergebirge, and (iii) for 100 years on a southeasterly exposed roof (370) in the Erzgebirge (Sachsen).

RESULTS AND DISCUSSION

The studied rock surfaces of unweathered (black) and weathered slates are fresh and undisturbed surfaces on cleavage planes. In this study, we compare the surface topography data of OM rich black slate with those of originally black slate, now nearly without OM due to its oxidative degradation. OM degradation is responsible for the rock's surface topography alteration (Fischer and Gaupp, 2005). The alum slate's OM has a shape of thin and small flakes. Figure 3 shows the size distribution of the OM flakes. Mostly they have a diameter of some microns or some tens of microns. The thickness of the flat OM flakes was not determined. Because no difference of the surface shape between black and weathered slates is visible by SEM, the OM height must be smaller than several microns. The black slate's OM shown in the figure is the residuum after treatment with fluoric acid (Fischer, 2002).

Alum Slate Surface Topography Alteration

Figure 4 shows VSI-measured height maps of the surfaces of a black, OM rich alum slate (A, sample #211) and of an oxidatively weathered alum slate that is nearly free of

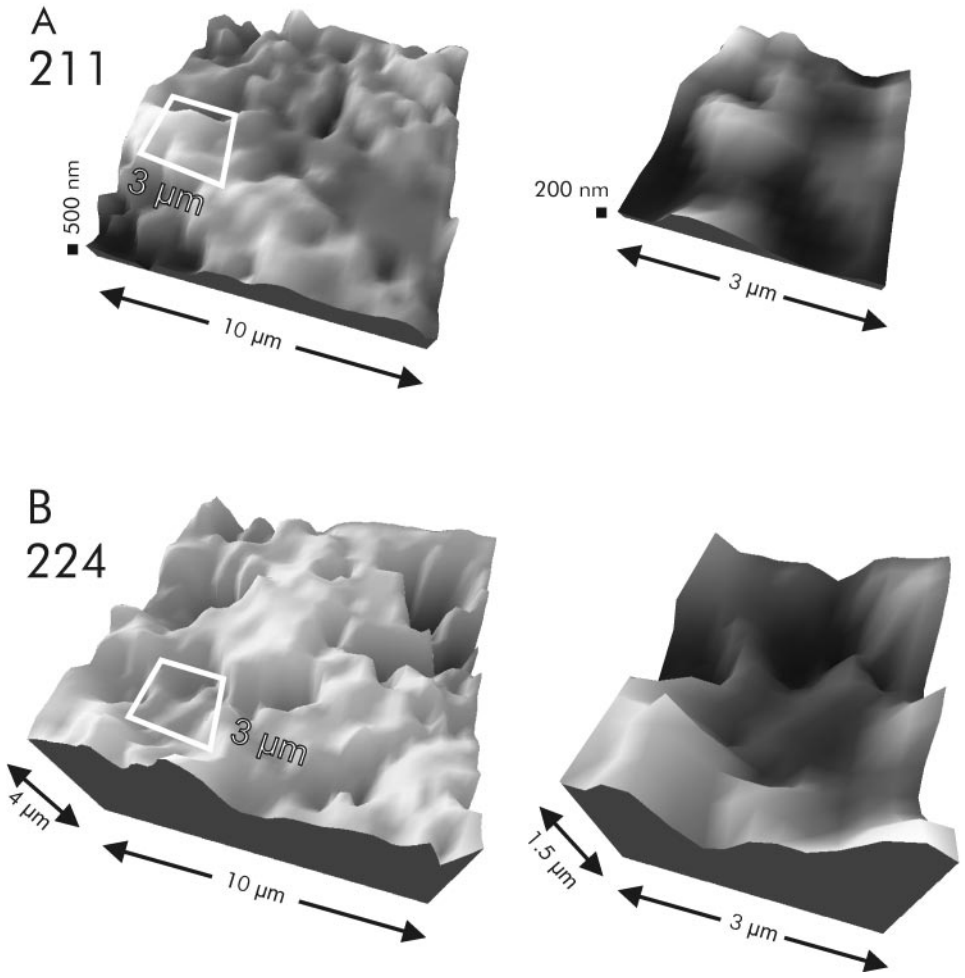

Fig. 4. VSI surface of a black alum slate (A, sample 211) and its white weathering product (B, sample 224). On the right side are shown sample sections with higher magnification.

OM (B, sample #224). Compared to the weathered slate, the OM rich slate shows a smooth surface with unevenness in the dimension of hundreds of nanometers. The weathered slate has a more uneven surface relief. Magnifications of surface sample sections shown at the right side of the figure underline these observations and show the occurrence of half-pores at the weathered rock surface in the micron range.

Surface topography parameters calculated from VSI data are presented in figure 5. *Rt* (A), *Rq* (B), *F* (C) are shown as a function of the sample length *a*. Those graphs show the existence of convergence (nearly constant values of surface topography parameters). *Rt* values of the weathered slate are converged for lateral extensions smaller than approximately 20 µm. According to the visualization of the extension of half-pores of weathered slate in figure 4B, the convergence (c1) breaks down for a sample length of 5 µm. *Rq* is converged with approximately 800 nm to 1 µm between 5 µm and 20 µm, too (# 224, c1). This standard deviation of surface height indicates a nearly constant peak-to-valley height. The maximum depth (= convergence of *Rt*) is approximately 7 µm. We conclude, the newly-formed half pores have nearly the same

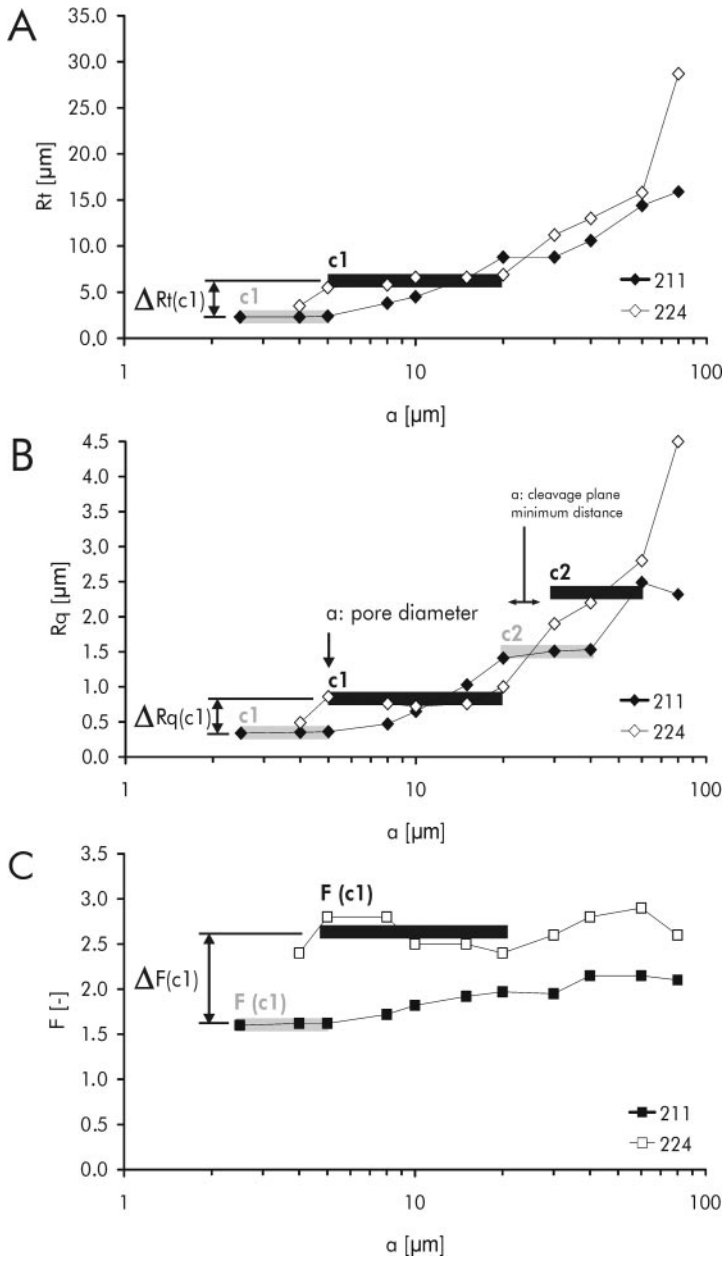

Fig. 5. Converged surface roughness parameter data, calculated from VSI data of black (sample 211) and white (sample 224) alum slates. Convergence is indicated by gray (black slate) or black (white slate) bars. The following parameters are shown: peak to peak height (*Rt*), surface roughness (*Rq*), and surface ratio (*F*).

lateral and vertical extension of ≥ 5 µm and < 7 µm, respectively. In contrast to the weathered slate, *Rt* and *Rq* of unweathered slate surfaces show convergence at sample axes lengths smaller than 5 µm. This supports our interpretation of a smooth unweathered slate surface with deviations in the range of 200 to 300 nm. In addition to

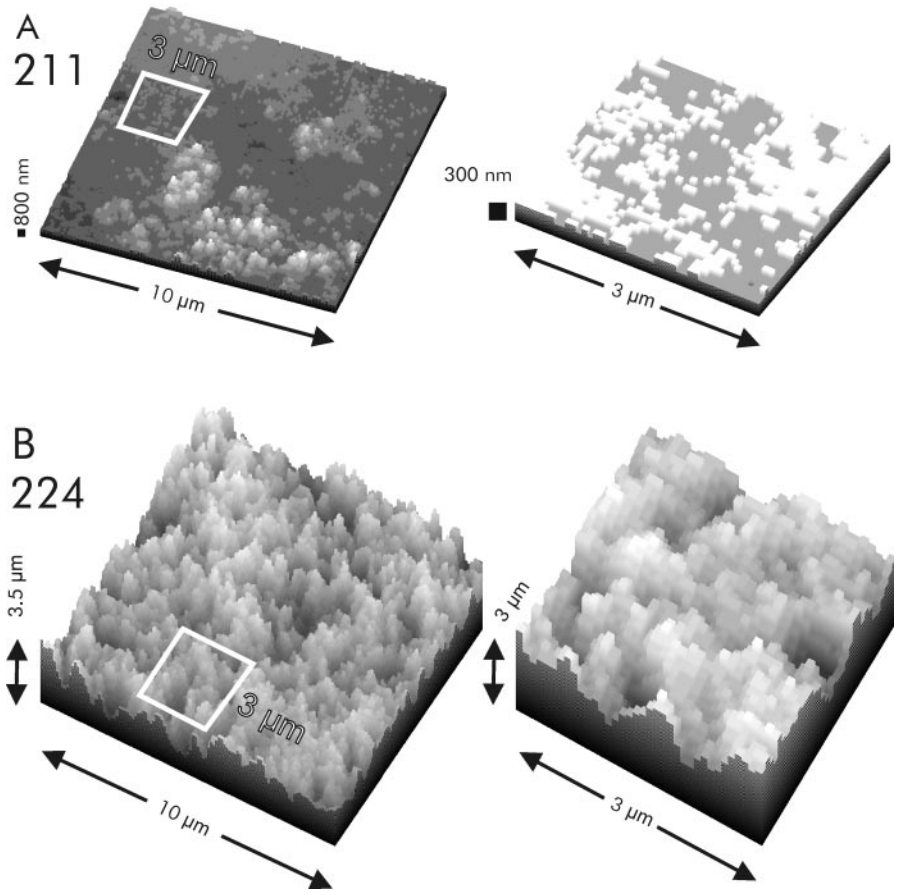

Fig. 6. LSM surface of a black alum slate (A, sample 211) and its white weathering product (B, sample 224). On the right side are shown sample sections with higher magnification.

the described features the slate samples show another surface component, dominating the *Rq* convergence plot of sample #211 between axes length of 20 µm to 50 µm. A flat slope of the Rq convergence graph for $a \approx 30$ to 60 µm is visible for sample # 224, also. Because this potential convergence exists for both, weathered and unweathered slate samples, this surface component responsible for convergence is not modified by weathering and represents most probably the size of sheet silicate aggregates (cleavage). The surface area ratio *F* of weathered slate samples is clearly higher than that of unweathered samples (fig. 5C). The differences between *F* values are not much affected by the convergence lengths mentioned above. The reason for this observation must be that in general it is the smallest surface component (pores with diameters smaller than the dimension of sheet silicate aggregates), which is responsible for the *F* value of the slate. Furthermore, the higher *F* value of weathered slate samples indicates the surface area magnification of the rock by OM decrease. This magnification is approximately 1.6 fold ($F_{weathered} \sim 2.5$, $F_{unweathered} \sim 1.6$ for convergence c1).

As a comparison, figures 4 and 6 show the same sample surface generated from VSI and LSM data, respectively. The corresponding surface topography parameters are shown in figure 7. The better lateral but lower vertical spatial resolution of LSM is

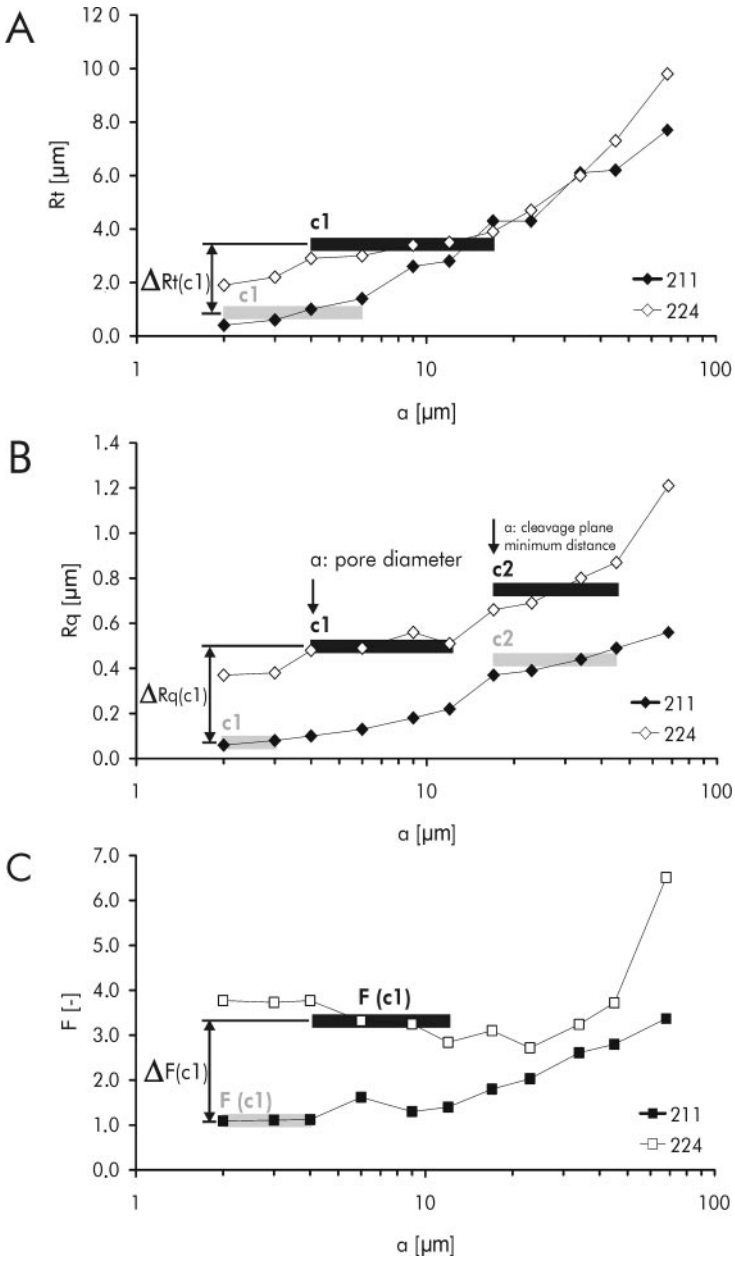

Fig. 7. Converged surface roughness parameter data, calculated from LSM data of black (sample 211) and white (sample 224) alum slates. Convergence is indicated by gray (black slate) or black (white slate) bars.

responsible for the visible differences in surface topographies shown in figures 4 and 6. A comparison of figure 6B (left) with figure 4 shows more lateral details of peaks and valleys of the weathered rock surfaces. As said above, the LSM measurements are able to detect steeply dipping flanks of surface components. Hence more individual components with a lateral extension smaller than 1 µm were detected with LSM. It is

likely that some of these components were amalgamated in the VSI data. In contrast, the strength of the VSI data is clearly shown by the differences of the same surface images in the right parts of figures 4 and 6. While VSI data can be used to detect surface height differences at the nanometer scale, the LSM image of the same surface shows a very simplified view of the height differences. As a consequence, the surface roughness parameters calculated from LSM data must be different—at least in part—compared to the same parameters calculated from VSI data.

Figure 7 shows surface roughness parameters calculated from LSM data. Convergence ranges of *Rt* and *Rq* values (figs. 7A and 7B) are similar to the VSI data results mentioned above. The lower vertical resolution is the reason for very low $F_{unweathered}$ values shown in the left part of figure 7C. For calculations of the surface area alteration during black slate weathering the $F_{unweathered}$ values (F(c1)) derived from VSI data are more realistic. In contrast, the higher $F_{weathered}$ values (F(c1)) derived from LSM data (fig. 7C) can provide more detailed information about the surface area increase caused by the decrease in organic matter. Based on these considerations, we estimate surface area increase caused by weathering of approximately 2.1 times ($F(\mathrm{c1})_{weathered\ (LSM)} \sim 3.3$, $F(\mathrm{c1})_{unweathered\ (VSI)} \sim 1.6$ for smallest axes lengths).

An alum slate weathering front of approximately 10 mm (Fischer and Gaupp, 2005) was investigated to detect surface parameter changes between the two final conditions (black slate, little or no OM decrease vs. white slate, nearly completely OM decrease). Three points of a weathering zone were analyzed by VSI, that is, a black and a white part as well as a dark gray transition zone between. Figure 8 (A-D) shows the surface parameter changes within this weathering zone. The highest peak-to-valley depths *Rt* were found for the gray slate. This result is equal to that of the *Rz* values (fig. 8D). Therefore, the gray slate part must have the highest relief differences. This result is not modified by parameter convergence. This consideration underlines the responsibility of small surface components that are significantly smaller than the axes length a of the sampled area for the surface topography and surface area differences between gray and black/white slate samples. From the ten-point height, *Rz*, we can estimate the dominating surface component height. Black slate samples show height differences smaller than ~1 μm, white slate samples smaller than ~2 μm, and gray slate samples smaller than ~3 μm (a = 5 μm). The standard deviation of these heights is relatively small for each slate type. Converged *Rq* data (fig. 8B, convergence between a = 5 μm and 8 μm for 211-white) are clearly smaller than 1 μm. F values of the gray slate surface are clearly higher than those of white and black slates (fig. 8C). It is plain that surface components with a lateral size of approximately 5 μm must be responsible for the total surface size of white and gray sample parts. In every case the F value of gray slate is larger than those of white or black slate samples. All these observations support the following model of surface area alteration during OM decrease (see also fig. 9): The aggregates of sheet silicates (mainly illite) that form the black slate are coated by organic matter. This coating causes a smooth surface with height differences at a range of hundreds of nanometers (black slates with initial OM content; fig. 9, left part). During oxidative OM decrease, pore spaces in the micron scale (a = 5 to 8 μm, *Rq* convergence of sample 211-white) are created. The newly-formed surface heights (peak valley heights), surface roughness, and the total surface area (F) are higher than those of the nearly completely OM free slate (fig. 9, right part). We conclude that the OM decrease in this rock follows the model shown in figure 9A rather than that in figure 9B. Model (B) requires an increase of the *Rt*, *Rz*, and F values caused by OM decrease from gray to white slate. Such an increase was not measured (fig. 8). Evidently, the comparison of gray slate and white slate data shows a clear decrease of all these surface parameters. In model (A), the OM degradation is faster in the "median" parts of the OM volume. Apparently the OM volume situated directly on the illite

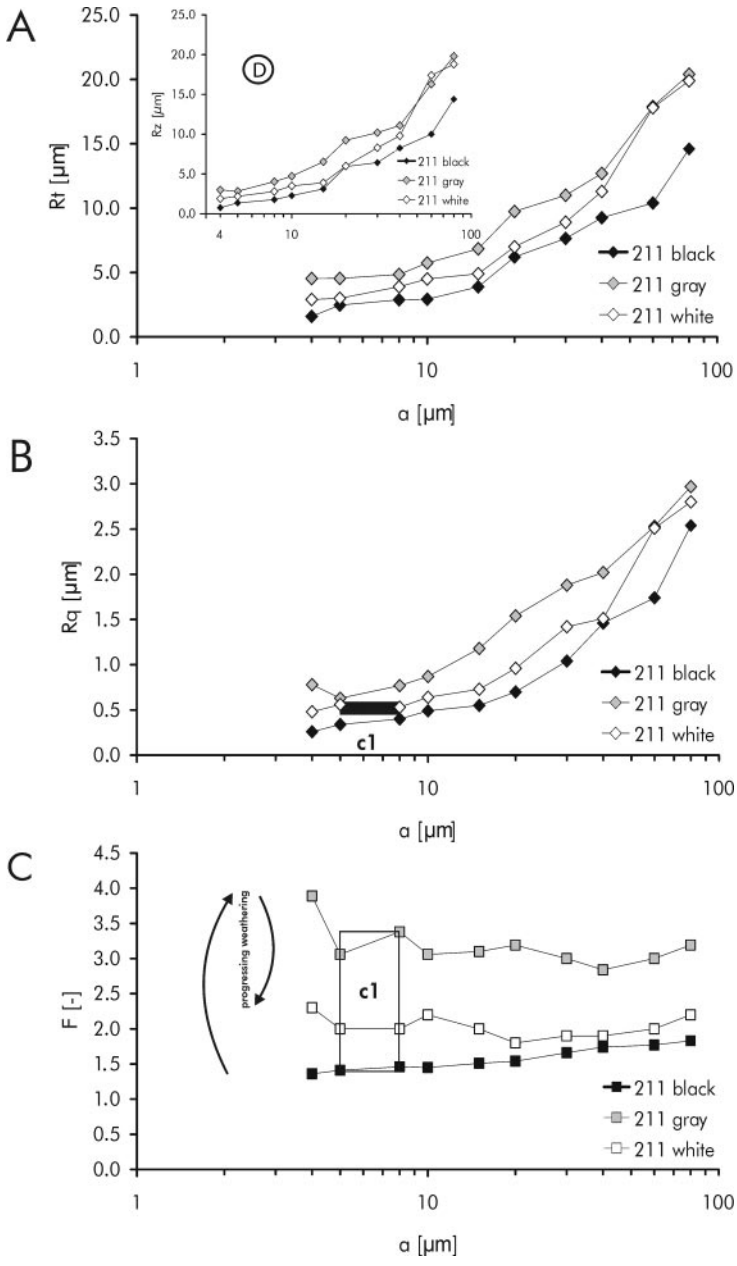

Fig. 8. Converged surface roughness parameter data of an alum slate weathering profile (progressing weathering: black, gray, white slate), calculated from VSI data. The following parameters are shown: peak to peak height (*Rt*), ten point roughness height (*Rz*), surface roughness (*Rq*), and surface ratio (*F*).

aggregates has a lower reactivity during oxidative weathering. We conclude that during ongoing OM weathering the rock surface reactivity and topography are controlled by the extent of OM degradation. Because both reactivity and topography of the observed surface will alter during reaction, it is obvious that an absolute term of "reactive" surface area must not be used to calculate the OM dissolution rates.

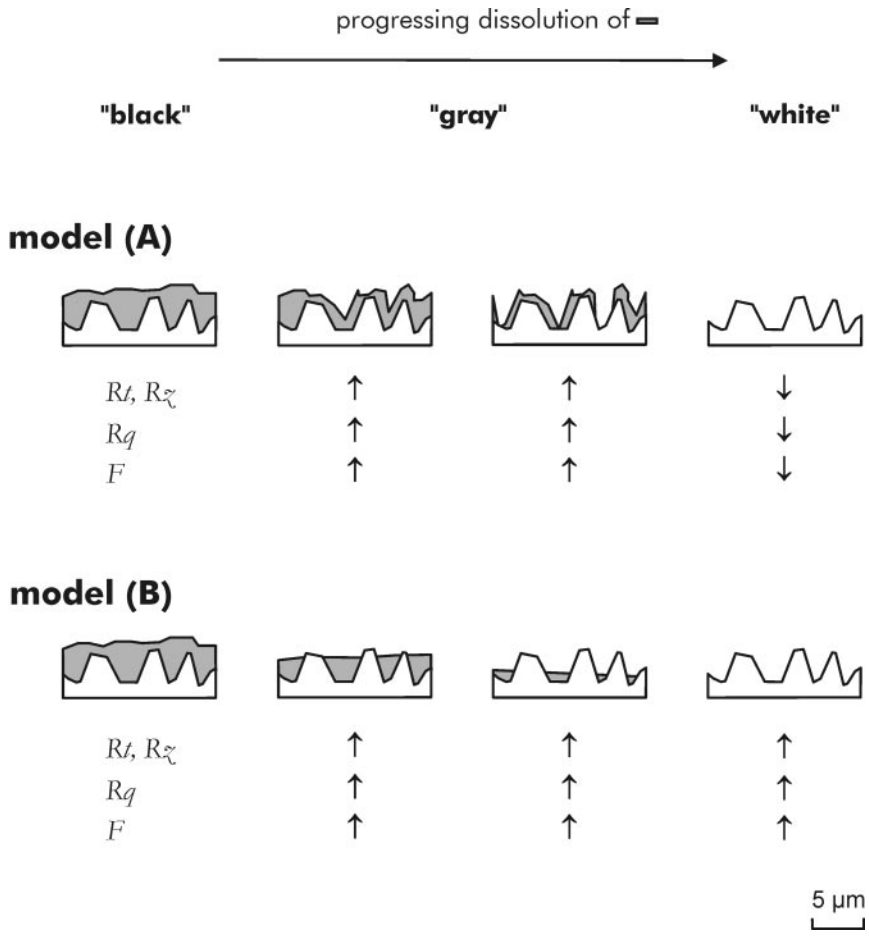

Fig. 9. Two models of OM degradation in black slates; model (A) illustrates the creation of OM intra pore space, model (B) shows a normal retreat of the OM volume.

Such a contrast in reactivity could have two causes: either there are different structural properties or there are different geochemical properties on the scale of a few microns. The first reason could be that sheet silicates have an influence on adjacent OM porosity or permeability. The other reason could be that OM consists of two separate chemical fractions having different reactivity. The latter reason was excluded for the OM investigated here (Fischer and others, 2007). In the alum slate an OM type was found that is uniform. The minor amounts of OM, remaining after intense weathering of black slates (gray, white samples) were not found to be more inert or to have higher maturity (thermal stability) compared to the OM of the not or slightly weathered, black slates.

Roof Slate Surface Topography Alteration

The second example of rock surface alteration by OM weathering highlights the surface parameter evolution of roof slates (Fischer and others, 2007). Two types of freshly mined roof slates (samples 399, 401) were compared to three weathered slates of the same lithotype but from different roofs (fig. 10). Two sections showing different

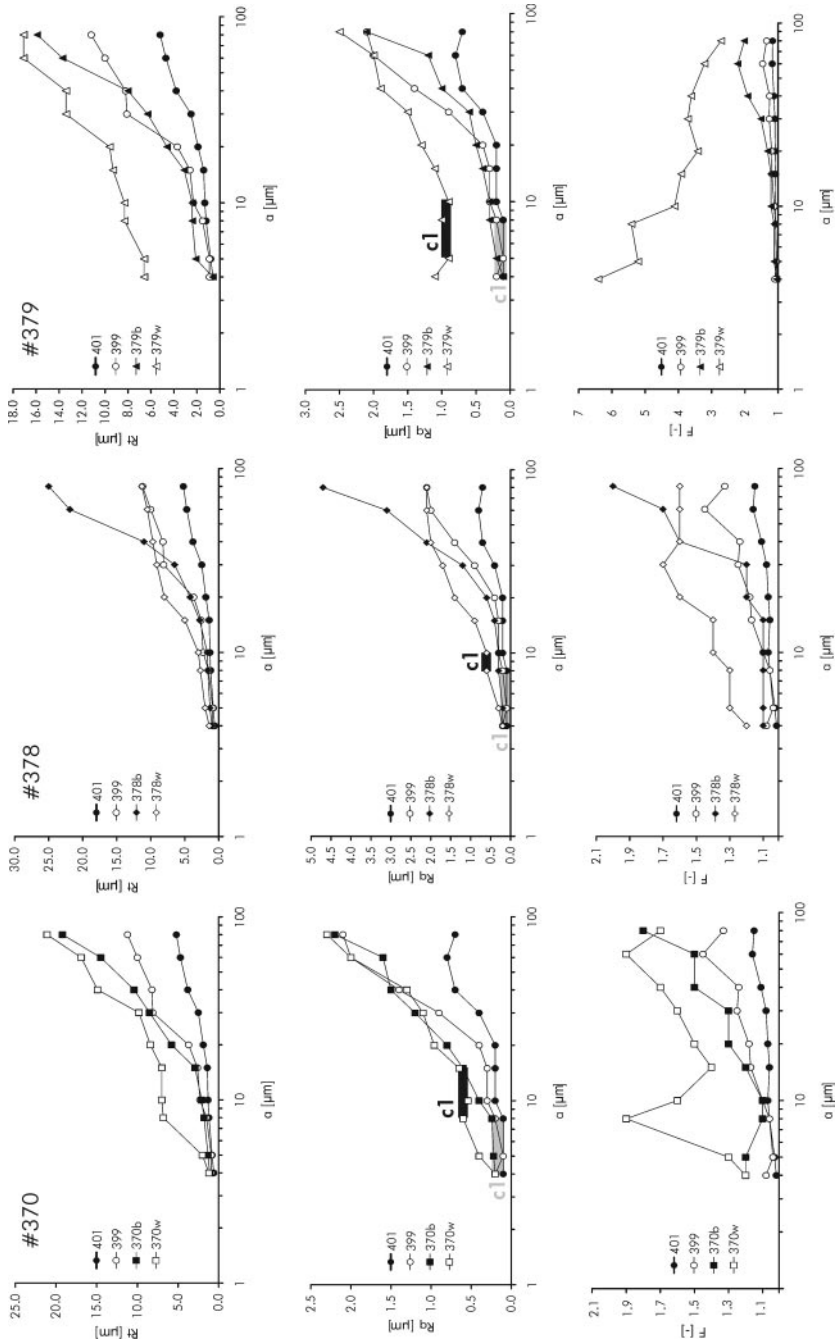

Fig. 10. Converged surface roughness parameter data, calculated from VSI data of fresh mined and weathered roof slates. The following parameters are shown: peak to peak height (*Rt*), surface roughness (*Rq*), and surface ratio (*F*). From each weathered roof slate the strongly weathered white part (w) and the less weathered black part (b) were analyzed. All data are compared to the data of the fresh mined slates (399, 401), respectively.

weathering intensities were analyzed by VSI (fig. 10, samples 370, 378, 379: b = black, w = white): The stronger weathered white part was directly exposed to surface weathering. The less weathered darker part of the roof slate was covered by the adjacent roof slate. These surface data and the data of the fresh slates were plotted in each diagram for comparison.

Freshly mined slates (399, 401) and slightly weathered slates (b-samples) show convergence of *Rq* for sample sections with axis lengths smaller than 8 μm. For larger sample sections the slate's surface relief is dominated by large surface components of different heights (large amounts of *Rt*, *Rq*). The surface area ratios (*F*) of samples 399 and 401 are relatively low (~1.1 – 1.3).

White roof slate samples (samples 370w, 378w, 379w) have a convergence range of *Rq* at approximately 5 to 15 μm. In this range, *Rt* and *Rq* data are clearly higher than those of unweathered slates and of the black, covered roof slate samples (samples 370b, 378b, 379b). The *Rt* and *Rq* data of black roof slate samples are very similar to those of the unweathered slates. We conclude that during strong weathering of roof slates (white parts), new pores are created with a diameter (peak-peak distance) of approximately 5 to 15 μm. The *Rt* data indicate, that the rock's surface shows half pores with a peak-valley height of ~ 8 μm (378w: only 4 μm). The creation of pore spaces within the black roof slates is clearly of little importance. The *Rt* and *Rq* data indicate a moderate pore space creation only.

This interpretation is supported by the *F* data of black roof slates that are similar to those of the fresh-mined slates. On the contrary, the *F* data of the white roof slates show clearly higher surface area ratios. Surface area ratio of sample 370w shows a maximum at sample length of 8 μm. This indicates that this surface component that dominates the rock surface area structure has a lateral extension of this length scale. In contrast, sample 379w shows no clear maximum value of *F* in the convergence graph. Because *F* increases with decreasing axis length, very small pores with diameters smaller than 4 microns must be responsible for the very large surface ratio. Sample 378w shows no distinct maximum in the convergence range of *Rt* and *Rq*. Therefore no single surface component of a certain size is dominating the rock surface area. These data demonstrate the creation of pores with different dimensions within the weathered roof slates. Because we compared rocks of the same lithotype, the diversity in the results indicates different weathering intensities of the roof slates. This is similar to the results from the alum slate weathering profile analysis (fig. 8), indicating the total rock surface area enlargement during the ongoing oxidative weathering. The surface area characterized here is the fluid-rock interface size. From BET and mercury intrusion porosity measurements it is known that the internal OM porosity will linearly decrease during oxidative degradation (Fischer and Gaupp, 2005). The results and interpretations presented here are therefore a helpful addition to understanding the reactivity of a rock component during weathering.

CONCLUSIONS

(1) The high spatial resolution in the z-direction and its broad field of view make light-optical topographic microscopy the ideal tool for observing rock surface alterations. The combination of vertical scanning interferometry and laser scanning microscopy offers the detection of surface elements with sizes of $x \sim y > 100$ nm and $z > 2$ nm.
(2) Convergence plots of statistical surface parameters offer the opportunity to detect differently sized components and their alteration on natural rock surfaces.
(3) Significant surface parameters for rock surface area characterization are the amplitude parameters *Rt* (peak-valley height), *Rz* (ten point surface height),

and *Rq* (root mean square roughness) as well as the surface relief area per measuring field ratio *F*; the latter characterizes the total interface area.

(4) The rock surface size evolution during dissolution of a certain component is traced by the change of converged amounts of *F*.

(5) The combination of converged *Rt*, *Rz*, *Rq*, and *F* data allows us to detect the predominance of surface normal retreat or of pore space creation during dissolution.

(6) The oxidative degradation of organic matter in black slates causes the alteration of an originally smooth surface (deviations of some hundreds of nm) to a rough surface with peaks and ridges in the scale of several microns.

(7) During the OM degradation process, the fluid–rock interface size increases. In contrast, progressive degradation with nearly complete OM degradation leads to a decrease in interface size. This indicates differences of the reactivity of OM during oxidative weathering.

ACKNOWLEDGMENTS

We thank I. Dunkl, V. Karius, H. Ruppert, and H. von Eynatten for helpful discussions. Many thanks to M. Baum (Schmiedebach-Lehesten), K. Müller (Schmiedefeld) and P. Fischer (Lauterbach) for slate samples. We would also like to thank two anonymous reviewers for very useful comments that significantly improved this manuscript. Thanks to C. Sturm for assistance with the English-language presentation. We gratefully acknowledge support for this study from the Deutsche Forschungsgemeinschaft (grant FI1212/1) and from the Alexander von Humboldt-Foundation (Feodor Lynen Fellowship to CF).

References

Arvidson, R. S., Ertan, I. E., Amonette, J. E., and Lüttge, A., 2003, Variation in calcite dissolution rates: A fundamental problem?: Geochimica et Cosmochimica Acta, v. 67, p. 1623–1634.

Ayebah, B., and Hung, Y. C., 2005, Electrolyzed water and its corrosiveness on various surface materials commonly found in food processing facilities: Journal of Food Process Engineering, v. 28, p. 247–264.

Blunt, L., 2003, Numerical Parameters for Characterisation of Topography, *in* Blunt, L., and Jiang, X., editors, Advanced Techniques for Assessment Surface Topography: London and Sterling, Virginia, Kogan Page Science, p. 17–41.

Blunt, L., Jiang, X., and Scott, P. J., 2005, Advances in micro and nano-scale surface metrology: Measurement Technology and Intelligent Instruments Vi, v. 295–296, p. 431–436.

Dong, W. P., Sullivan, P. J., and Stout, K. J., 1992, Comprehensive Study of Parameters for Characterizing 3-Dimensional Surface-Topography .1. Some Inherent Properties of Parameter Variation: Wear, v. 159, p. 161–171.

——— 1993, Comprehensive Study of Parameters for Characterizing 3-Dimensional Surface-Topography .2. Statistical Properties of Parameter Variation: Wear, v. 167, p. 9–21.

——— 1994a, Comprehensive Study of Parameters for Characterizing 3-Dimensional Surface-Topography .3. Parameters for Characterizing Amplitude and Some Functional-Properties: Wear, v. 178, p. 29–43.

——— 1994b, Comprehensive Study of Parameters for Characterizing 3-Dimensional Surface-Topography .4. Parameters for Characterizing Spatial and Hybrid Properties: Wear, v. 178, p. 45–60.

Dove, P. M., and Platt, F. M., 1996, Compatible real-time rates of mineral dissolution by Atomic Force Microscopy (AFM): Chemical Geology, v. 127, p. 331–338.

Eggleton, R. A., and Busek, P. R., 1980, High resolution electron microscopy of feldspar weathering: Clays and Clay Minerals, v. 28, p. 173–178.

Fischer, C., 2002, Oberflächenquantifizierung an Schwarzpeliten unterschiedlicher Verwitterungsgrade: Jena, Germany, Institut für Geowissenschaften, Friedrich-Schiller-Universität Jena, p. 117 + 37.

Fischer, C., and Gaupp, R., 2005, Change of black shale organic material surface area during oxidative weathering: Implications for rock-water surface evolution: Geochimica et Cosmochimica Acta, v. 69, p. 1213–1224.

Fischer, C., and Koch, A., 2005, Die Porenraumentwicklung eines schwarzen Dachschiefers bei oxidativer Verwitterung: Zeitschrift der Deutschen Gesellschaft für Geowissenschaften, v. 156, p. 75–79.

Fischer, C., Karius, V., and Thiel, V., 2007, Organic matter in black slates shows oxidative degradation within only a few decades: Journal of Sedimentary Research, v. 77, p. 355–365.

Hamilton, D. K., and Wilson, T., 1982, Three-dimensional surface measurement using the confocal scanning microscope: Applied Physics, v. 27, p. 211–213.

Helgeson, H. C., Murphy, W. M., and Aagaard, P., 1984, Thermodynamic and kinetic constraints on reaction rates among minerals and aqueous solutions. II. Rate constants, effective surface area, and the hydrolysis of feldspar: Geochimica et Cosmochimica Acta, v. 48, p. 2405–2432.
Hochella, M. F., and White, A. F., 1990, Mineral-Water Interface Geochemistry—an Overview: Reviews in Mineralogy, v. 23, p. 1–16.
IUPAC, 1994, Recommendations for the characterization of porous solids: Pure and Applied Chemistry, v. 66, p. 1739–1758.
Jorgensen, J. F., Carneiro, K., and Madsen, L. L., 1993, The scanning tunneling microscope and surface characterization: Nanotechnology, v. 4, p. 152–158.
Karcz, Z., Aharonov, E., Ertas, D., Polizzotti, R., and Scholz, C. H., 2006, Stability of a sodium chloride indenter contact undergoing pressure solution: Geology, v. 34, p. 61–63.
Lasaga, A. C., and Blum, A. E., 1986, Surface chemistry, etch pits and mineral-water reactions: Geochimica et Cosmochimica Acta, v. 50, p. 2363–2379.
Lion, M., Ledesert, B., Skoczylas, F., Recourt, P., and Dubois, T., 2004, How does micropetrography help us to understand the permeability and poromechanical behaviour of a rock?: Terra Nova, v. 16, p. 351–357.
Littke, R., Klussmann, U., Krooss, B., and Leythaeuser, D., 1991, Quantification of loss of calcite, pyrite, and organic-matter due to weathering of Toarcian black shales and effects on kerogen and bitumen characteristics: Geochimica et Cosmochimica Acta, v. 55, p. 3369–3378.
Lüttge, A., Bolton, E. W., and Lasaga, A. C., 1999, An interferometric study of the dissolution kinetics of anorthite: The role of reactive surface area: American Journal of Science, v. 299, p. 652–678.
Lüttge, A., Winkler, U., and Lasaga, A. C., 2003, Interferometric study of the dolomite dissolution: A new conceptual model for mineral dissolution: Geochimica et Cosmochimica Acta, v. 67, p. 1099–1116.
Metz, V., Raanan, H., Pieper, H., Bosbach, D., and Ganor, J., 2005, Towards the establishment of a reliable proxy for the reactive surface area of smectite: Geochimica et Cosmochimica Acta, v. 69, p. 2581–2591.
Pfeiffer, H., Blumenstengel, H., and Wiefel, H., 1995, Dinant (Unterkarbon), *in* Seidel, G., editor, Geologie von Thüringen: Stuttgart, E. Schweizerbartsche Verlagsbuchhandlung, p. 147–166.
Rothenhöfer, P., Sahin, H., and Peiffer, S., 1999, Attenuation of heavy metals and sulfate by aluminium precipitates in acid mine drainage?: Acta Hydrochimica et Hydrobiologica, v. 28, p. 136–144.
Stout, K. J., 1993, Development of Methods for the Characterisation of Roughness in Three Dimensions: London, Penton Press, 358 p.
Thomas, T. R., 1999, Rough Surfaces: London, Imperial College Press, 278 p.
White, A. F., and Brantley, S. L., 1995, Chemical weathering rates of silicate minerals: An overview, *in* White, A. F., and Brantley, S. L., editors, Chemical Weathering Rates of Silicate Minerals: Reviews in Mineralogy, v. 31, p. 1–22.